




Experimental investigation of preferential concentration in zooplankton swimming in turbulence

François-Gaël Michalec^{1,a} , Olivier Praud², Sébastien Cazin², and Eric Climent²

¹ Univ. Lille, CNRS, Univ. Littoral Côte d'Opale, UMR 8187 LOG, Laboratoire d'Océanologie et de Géosciences, Station marine de Wimereux, 59000 Lille, France

² Institut de Mécanique des Fluides de Toulouse, UMR 5502, Université de Toulouse, CNRS, 31400 Toulouse, France

Received 31 August 2021 / Accepted 20 January 2022 / Published online 7 February 2022

© The Author(s), under exclusive licence to EDP Sciences, SIF and Springer-Verlag GmbH Germany, part of Springer Nature 2022

Abstract Turbulence can cause particles to accumulate within specific regions of the flow. One mechanism responsible for this phenomenon, called preferential concentration, consists in particle–fluid interactions yielding inhomogeneous spatial distribution of particles into clusters or depleted regions due to density difference or finite-size effects. In the case of living particles such as plankton, clustering may also originate from their motility or from their behavioral response to turbulent forcing. Preferential concentration of plankton has attracted much attention, because it is a key determinant of encounter rates and therefore relevant for a wide range of ecological processes. However, most studies have focused on microscopic cells, and consequently the case of larger organisms remains poorly studied. Here, we use high-performance particle tracking and three-dimensional Voronoï analysis to test for the emergence of clustering in the spatial distribution of calanoid copepods, the most important metazoans in the oceans in terms of biomass. We found that neither inertia nor motility resulted in significant departure from a random Poisson process over a range of turbulence intensity from very strong to moderate. However, we observed weak clustering in calm water, which may originate from hydrodynamic and olfactory interactions between organisms. Our results improve our understanding of fluid–particle interactions in the zooplankton and have important implications for the modeling of their encounter rates in turbulence.

1 Introduction

Plankton often encounter turbulence in their habitats, and how turbulence influences their ecology is a domain of intensive research. The coupling between the hydrodynamic forces generated by turbulence and the shape, size, density, and motility of plankton results in a diversity of responses that have important implications for ecosystem functions and processes. Examples include the interaction between shear and the body asymmetry of some motile phytoplankton, which can disrupt their vertical migration [16], or the active behavioral response of invertebrate larvae to specific hydrodynamic signals, which allows them to regulate their vertical position in the water column to reach favorable locations [24].

In turbulence, particles that have a different density than the carrier fluid and/or a finite size can accumulate within specific regions of the flow. This phenomenon is referred to as preferential concentration. It has been intensively studied, because it is relevant for a wide range of industrial and environmental issues, for instance the combustion of oil droplet sprays, the for-

mation of rain droplets, or the encounter rates of planktonic organisms [7, 58]. For the case of particles that are heavy and much smaller than the dissipative scale of the flow, the tendency to distribute non-uniformly is attributed to their centrifugation by turbulent vortices and their accumulation within regions of high strain rate [26, 60]. This phenomenon is controlled by the dimensionless Stokes number, the ratio of the particle viscous relaxation time to a turbulent time scale (usually the Kolmogorov time scale), which determines how faithfully a particle follows fluid elements. With an appropriate definition, Stokes numbers close to unity correspond to the strongest preferential concentration both for heavy and light particles [4, 66]. Accumulation of small and light particles within regions of high vorticity is driven by added-mass effects that act as a centripetal force toward vortex cores [62]. When particles are motile, as in the case of many species of plankton, preferential concentration can also result from the interactions between the hydrodynamic forces generated by turbulence and the swimming behavior and morphology of the organisms. The focus has generally been on microscopic phytoplankton cells, and most of what we know on this topic derives from theoretical work or numerical simulations exploring the influence of various parameters such as shape or swimming velocity

^a e-mail: francoisgael.michalec@univ-lille.fr (corresponding author)

on the emergence of clustering [22, 51]. For instance, at the microscale, the coupling between motility, velocity gradients, and the stabilizing torque that some phytoplankton use to direct their vertical motion can drive intense patchiness in their distribution, increasing the local cell concentration by several orders of magnitude compared to non-motile organisms [12, 15].

Much less is known about zooplankton. These organisms play fundamental roles in aquatic ecosystems from lakes to estuaries to the ocean. Located at the base of the food web, they channel nutrients and energy from the primary producers to higher trophic levels [57], they support the development of larger animals including commercially important fishes [3], and they form an important component of the biological carbon pump [59]. Previous experimental work and numerical simulations have shown that particles with a size larger than or comparable to the dissipative scale of turbulence and a density larger than that of the fluid tend to cluster in strain-dominated regions of the flow [21, 27] or in the vicinity of zero-acceleration points of the flow [10]. However, information is scarce for particles with a size larger than or comparable to the dissipation scale of the flow and a density close to that of the carrier fluid, which is the case of many zooplankton. This limits our ability to predict the prevalence of zooplankton clustering in the environment and to understand its influence on their ecology.

Clustering of zooplankton may result from the interactions between turbulence and their morphology. Earlier theoretical work and numerical simulations have suggested that clustering due to finite-size and density may be ecologically significant for zooplankton, because it can increase the probability for two organisms to be within their perception radius, thereby increasing encounter rates [35, 55, 58]. The elongated shape of many species of zooplankton may contribute further to clustering, because shape effects add to inertial effects [40]. In addition, preferential concentration may also result from the behavioral response of the organisms to hydrodynamic stress generated by the flow. Indeed, some zooplankton such as copepods can detect and react to hydrodynamic signals in their vicinity by performing escape reactions directed away from the disturbance [19]. Several studies indicate that the hydromechanical stimulus that triggers escape jumps is the presence of flow velocity gradients [33], which copepods detect via the bending of the mechanoreceptors located on their first antennae [69]. During these escape reactions, copepods reach very high velocities, above 100 mm/s for *Eurytemora affinis*, the species studied in the present work (body length of approx. 1 mm) [6, 45]. Important insights have been gained from numerical simulations that have inferred on the role of these jumps in the emergence of clustering in turbulence. The rationale is that by moving away from regions of high strain rate via escape jumps, organisms may accumulate in some specific regions of the flow [1, 2]. In these simulations, clustering was observed for a specific range of jump amplitudes and shear rate thresholds. However, there is a lack of experimental data to confirm

these previous theoretical or numerical studies, primarily because of the difficulties of observing at appropriate spatial and temporal scales the motion of many organisms swimming simultaneously in turbulence.

In the present study, we test experimentally for the existence and extent of preferential concentration due to physical effects (particle size, inertia, and elongated shape) and behavior in a suspension of calanoid copepods swimming freely in turbulence. We reconstruct the trajectories of thousands of copepods swimming simultaneously in a large volume by means of three-dimensional particle tracking velocimetry. We study their concentration field using Voronoï diagrams, a robust technique to detect and quantify clustering [21]. The paper is organized as follows. First, we present the experimental setup and the methodology to reconstruct the trajectories of the organisms in 3D. Flow conditions from calm water to strong turbulence have been tested and characterized by means of particle image velocimetry. Second, we discuss the results on swimming velocity and preferential concentration of copepods under these flow conditions. More specifically, we compare the ratio of the probability density function of the velocity of living copepods to that of inert carcasses to quantify the behavioral response of copepods to a sudden increase in turbulence. We observe a substantial increase in this ratio for swimming velocities corresponding to escape jumps. Then, we compare the deviation of the probability density function of the normalized volume of the Voronoi cells to that of randomly distributed particles to test for the emergence of preferential concentration due to inertia and to escape jumps in turbulence and calm water. In the last section, we interpret our findings in light of previous results from the literature and draw conclusions.

2 Materials and methods

Our experimental measurements presented a number of technical challenges mainly associated with the reconstruction of the trajectories of many organisms swimming simultaneously in a large investigation volume at a concentration dense enough to obtain reliable statistics. In this section, we present in detail our experimental conditions and data processing based on our experience in 3D particle tracking and with measuring zooplankton behavior.

2.1 Organisms

The species used in our measurements is the calanoid copepod *Eurytemora affinis*. Copepods represent the main component of the meso-zooplankton in brackish and marine ecosystems and the most important metazoans in the oceans and in estuaries in terms of biomass. These small crustaceans play pivotal roles in aquatic ecosystems by contributing to the transfer of carbon and energy from the phytoplankton to higher trophic levels. *E. affinis* is a widespread and ecologically rele-

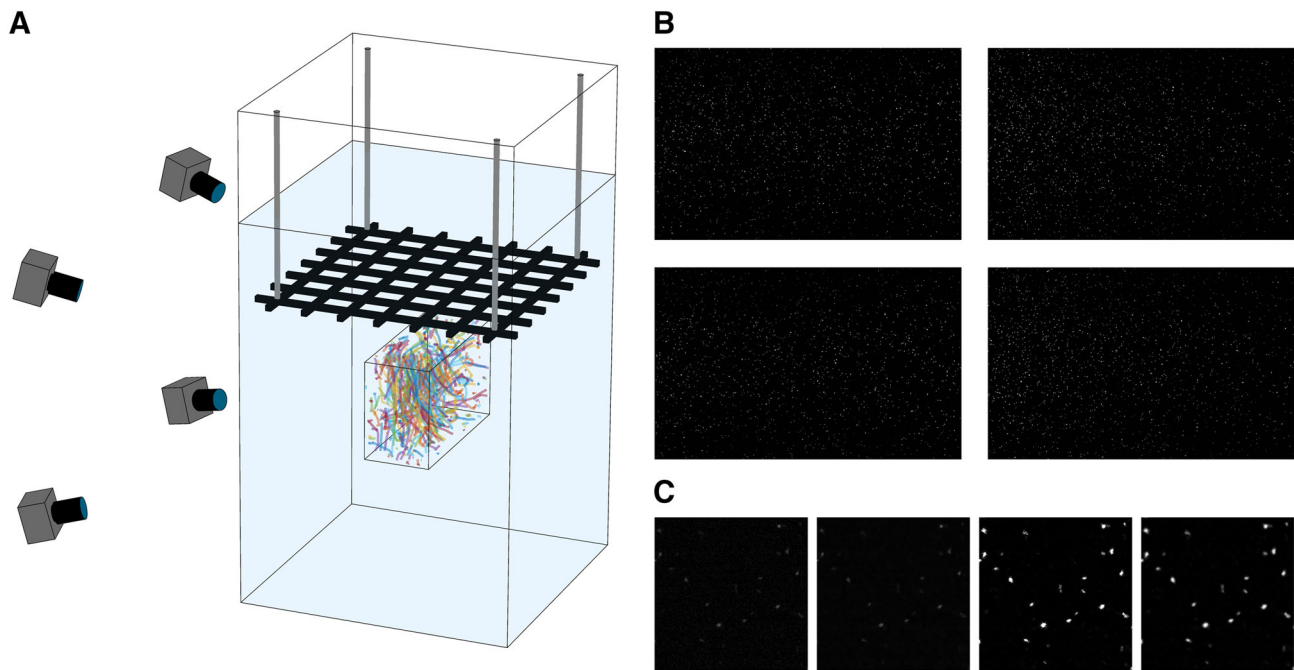


Fig. 1 Copepod tracking in 3D. **A** Sketch of the experimental setup. Four synchronized cameras recorded plankton motion from one side of the aquarium. The investigation volume was located in the middle of the tank, 10 or more cm away from the walls. This large distance precluded wall effects. Illumination was provided by two panels of infrared diodes located on the sides of the tank (not shown for clar-

ity). **B** Typical images from the four cameras, for a single time step, after pre-processing. Copepods appear as bright particles on a dark background. **C** Close-up on one image, showing the effects of image pre-processing to improve the detection of copepods. From left to right: original image, after adaptive noise-removal filtering, after contrast stretching, and after Gaussian blurring

vant species. It often dominates the zooplankton community by biomass in the low-to-medium salinity zone of several major European and North-American estuaries, where it represents an important component of the food web, and it is also found in lakes and in the Baltic sea [13, 31]. Copepods, microalgae (*Rhodomonas baltica* and *Isochrysis galbana*) to feed the copepods, and seawater were obtained from the group of S. Souissi at Lille University [11]. Measurements were performed at the *Institut de Mécanique des Fluides de Toulouse*, within a few days after receiving the organisms.

2.2 Turbulence generation

The experimental tank was 50 cm (L) by 50 cm (W) by 90 cm (H). The flow was forced by the vertical motion of a grid (beam width 10 mm, mesh size 45 mm) driven by a servomotor mounted on top of the tank [18] (Fig. 1A). Turbulence was initiated by a single pass of the grid from the bottom of the tank to the top, at a speed of 150 cm/s. The recording started once the grid reached the top and lasted over the free decay of the turbulence (3500 frames, corresponding to approx. 11.67 s).

2.3 Turbulence quantification

The turbulence after the pass of the grid was measured during preliminary measurements (i.e., without cope-

pods) by means of particle image velocimetry (PIV), using in-house software. The flow was seeded with hollow glass spheres with a diameter $d_p = 10 \mu\text{m}$ and a material density $\rho_p = 1.10 \text{ g/cm}^3$. Their Stokes number decreases from 9×10^{-5} after the pass of the grid to 3.4×10^{-5} at the end of the decay because of the increase in the Kolmogorov length scale η , which indicates that they behaved as passive tracers. The Stokes number is given by $St = \tau_p / \tau_\eta = (1/18) (\rho_p / \rho_f) (d_p / \eta)^2$ where τ_p is the particle relaxation time, τ_η is the Kolmogorov time scale, and ρ_f is the density of the fluid. This definition corresponds to the conventional Stokes number and is valid for particles much smaller than η [67]. The velocity of the flow tracers was measured in a vertical plane (17 cm by 17 cm) perpendicular to grid face, in the center of the tank. The investigation domain was illuminated by a light sheet from a Nd:Yag laser delivering 200 mJ per pulse. A pco.2000 camera (PCO) recording at a resolution of 2048 by 2048 pixels was mounted in front of the investigation domain. The recording frequency of the image pairs was 5 Hz. The separation time between images of the same pair varied over the duration of the recording to ensure that the average particle displacement was roughly one fourth of the size of the final interrogation window. A total of 100 statistically independent replicates was processed, with 50 image pairs recorded per replicate. Images were processed using a standard PIV algorithm. A three-pass process

with an interrogation window ranging from 64 to 32 pixels and with a window overlap of 50 % was used. Spurious vectors were identified following each iteration via global and local median filters and replaced by a linear interpolation of the surrounding vectors. The resulting flow field has velocity vectors separated by 15 pixels in the horizontal and vertical directions, which corresponds to a spatial resolution of approx. 1.24 mm (from 4.8η after grid pass to 3η at the end of the decay).

2.4 Measurements with copepods

We recorded copepod motion using a stereovision system composed of four synchronized Phantom VEO 640L (Vision Research) recording at 300 Hz and at a resolution of 2560 by 1600 pixels. The cameras were equipped with macro 100 mm lenses (Zeiss) mounted on LaVision Scheimpflug V3 adaptors. Illumination was provided by two panels of infrared diodes (GS-VITEC MultiLED LT, 850 nm, 50 W) so as not to trigger phototaxis, since *E. affinis* displays positive directional response to visible light. We reconstructed copepod trajectories by means of three-dimensional particle tracking velocimetry (3D-PTV), using the open-source software OpenPTV (OpenPTV Software Consortium, <http://www.openptv.net>). This technique identifies and follows individual particles in time and provides a Lagrangian description of their motion in 3D. It was originally developed to measure turbulence [37–39, 65] and it has been previously adapted to study the swimming behavior of small aquatic organisms [43, 56]. To study the emergence of preferential concentration, we imaged the distribution of copepods within a volume of 29 cm (L) by 18 cm (H) by 12 cm (W) located in the middle of the experimental tank. The concentration was approx. 400 copepods per liter. This concentration is dense enough to obtain reliable statistics and comparable to values observed in estuaries where the number density can reach 600 copepods per liter or even more [14]. We filled the experimental tank with water at salinity 15 (seawater from the English Channel adjusted to salinity with distilled water) and at 18° C. The water was filtered through 0.2 μm cartridges to remove impurities responsible for light scattering and attenuation. Copepods were gently transferred from the cultures to the tank and let to acclimate for approx. one hour. We recorded the motion of living copepods in still water (three consecutive recordings of 3500 images each) and during the decay of turbulence (five consecutive recordings, each preceded by a single pass of the grid, with a one-minute delay between recordings). Only adults and late copepodite stages were used (size fraction above 300 μm), because younger developmental stages do not have the swimming capabilities of adults and therefore cannot self-propel efficiently in turbulence. We also performed identical measurements using dead copepods (two consecutive recordings) as a reference case. Copepods were checked visually after grid pass and were

found swimming actively within the tank with no sign of damage.

2.5 Image pre-processing and trajectory reconstruction

Because of the large experimental tank, the strong attenuation of near-infrared wavelengths in salty water, and the reduced sensitivity of the sensors to infrared wavelengths, copepods appeared in the images as dim particles on a noisy dark background (Fig. 1B). To improve their detection, we filtered the images with a linear adaptive filter that removed background noise and we performed a contrast stretching transformation that lowered the intensity of the background and increased that of the copepods. The center of the particles was then determined with subpixel accuracy for each copepod as the center of mass of all the bright pixels surrounding one local maximum. To reduce the noise in the determination of these centers, we added a slight Gaussian blur to the images (Fig. 1C). Image pre-processing was done using in-house MATLAB code. Then, using the OpenPTV software, we calibrated the cameras using a calibration plate with dots of known coordinates imaged at different positions along the optical axis, and we performed an additional dynamic calibration based on the images of moving particles [36]. Knowing the camera intrinsic and extrinsic parameters, the software established correspondences between particle image coordinates across multi-camera views using the epipolar line intersection technique and retrieved the 3D positions of the moving particles from the collinearity equations. Copepods were then tracked using an algorithm based on image and object space information [37–39, 65]. We were able to track individual copepods down to a separation distance of approx. 1 mm (separation between the centroids of two adjacent particles). This value corresponds to one body length of an adult *E. affinis* and is the minimal distance at which two closely interacting copepods with complex shape and motion could be tracked reliably. This means that two copepods whose centroids are separated by 1 mm are actually in close contact and that our particle tracking technique is able to detect clustering down to the shortest scales.

2.6 Trajectory post-processing

Reconstructed trajectories were post-processed using in-house MATLAB code. First, spurious trajectories were filtered out based on the particle displacement. These short, non-significant trajectories typically result from impurities in the water, bright elements in the image background, or reflections on the surface of the aquarium. Second, segments belonging to the same broken trajectory were detected and connected by applying a predictive algorithm that uses the position, velocity, and acceleration of the particles along their trajectories [42]. Broken trajectories typically occur because of occlusion or, in the case of copepods, because of their

intermittent jumps that challenge most particle tracking algorithms. Third, trajectories were smoothed with a third-order polynomial filter with a width of 21 points, corresponding to the Kolmogorov time scale τ_η immediately after the pass of the grid and to $0.4 \tau_\eta$ at the end of the recording. This value represents a good compromise between improving the determination of the coordinates and their derivatives while preserving the features of the data, especially the strong velocity fluctuations that result from the frequent jumps of copepods [44]. The velocity and acceleration of the copepods were directly obtained from the coefficient of the polynomials. We obtained more than 10^7 data points for living copepods in calm water, more than 3.7×10^7 data points for living copepods in turbulence, and more than 1.5×10^7 data points for dead copepods in turbulence. For each sequence, the number of detected copepods remained roughly constant in time during the recording duration.

2.7 Clustering analysis

The aim was to study the local concentration field in order to quantify clustering due to inertia and swimming behavior, if any. The concentration field was investigated by means of Voronoï diagrams. This technique has been used in turbulence research to quantify with high robustness the emergence of preferential concentration of water droplets in a turbulent airflow [46] and the clustering of finite-size particles and air bubbles in turbulent fluid flows [21, 62]. A Voronoï diagram represents a three-dimensional tessellation performed on a set of particles; each cell of the tessellation is linked to a particle in that it includes all points closer to it than to any other particle in the set. The volume of each cell is therefore the inverse of the local particle concentration at a scale corresponding to the separation distance between the particles. To compare results from measurements conducted with different numbers of copepods, the volume V of each cell is normalized by the average volume of the cells $\langle V \rangle$, which is independent of the spatial distribution of the particles [20]. We tested for preferential concentration by comparing the probability density function (PDF) of the normalized volume of Voronoï cells to that of randomly distributed particles, whose shape is well approximated by a Gamma distribution. The deviation of the normalized PDF provides a quantification of the intensity of clustering. We used the analytical expression of Ferenc and Nédá as a reference for the shape of the PDF for particles distributed as a random Poisson process [20].

Voronoï diagrams were calculated for each time step and each recording. Then, recordings were divided into 5 sequences of 700 frames each (corresponding to approx. 2.33 s), referred to as S1 to S5. The PDF of the normalized cell volume was constructed for each sequence after pooling the data from the different recordings of the same experimental condition (living copepods in calm water, living copepods in tur-

bulence, and dead copepods in turbulence). The first sequences, immediately after the pass of the grid, correspond to intense turbulence (see the next section for a presentation of the turbulence quantities). The time- and space-averaged turbulent kinetic energy dissipation rate ε ranges from $2.7 \times 10^{-4} \text{ m}^2/\text{s}^3$ during S1 to $7.6 \times 10^{-5} \text{ m}^2/\text{s}^3$ during S2. These values are above those measured in the ocean, where ε typically ranges from $10^{-8} \text{ m}^2/\text{s}^3$ below the mixed layer to $10^{-4} \text{ m}^2/\text{s}^3$ near the surface [61]. Similarly, the Taylor-scale Reynolds number Re_λ ranges from 269 to 277, whereas typical environmental values correspond to $Re_\lambda = O(10^2)$. These conditions are not likely to be encountered by copepods in typical environmental conditions [23]. However, they are appropriate to detect clustering due to the Stokes number of the particles, as in general preferential concentration increases with the Reynolds number [62]. Indeed, copepods have an elongated shape (aspect ratio is approx. 3 for *E. affinis*), are slightly heavier than seawater [34], and in our measurements their size d_p is comparable to or larger than the Kolmogorov length scale η (d_p/η ranges from 3.8 in S1 to 2.4 in S5). Their conventional Stokes number St , i.e., the ratio between particle viscous relaxation time and the Kolmogorov time scale τ_η , is close to unity at the highest turbulence intensity tested in our measurements ($St \cong 0.8$). This value is much larger than for tracers. Therefore, one may expect copepods to depart from the flow streamlines and to accumulate within specific regions of the flow because of their Stokes number, irrespectively of their behavior. Indeed, previous experimental work has indicated that the velocity and acceleration statistics of dead copepods differ substantially from those of tracers [42, 43]; however the influence of St on the local concentration field is not well known. The intense turbulence in the first sequences sets an upper bound to observe clustering due to St . The last sequences correspond to weaker turbulence. In these sequences, flow velocity fluctuations are moderate (16 mm/s in S5), comparable to those measured in the field [50, 68], and below the velocities reached by *E. affinis* during jumps [42]. The measured energy dissipation rate ($3.3 \times 10^{-5} \text{ m}^2/\text{s}^3$) is comparable to values measured in turbulent environments inhabited by *E. affinis* such as coastal areas and estuaries where most of the turbulence originates from tidal forcing instead of wind [50]. Therefore, the first sequences are appropriate to test for the existence and extent of clustering due to inertia alone, while the last sequences are appropriate to test for the contribution of motility and to the behavioral response of copepods to the local flow field, combined with inertia [1].

3 Results

3.1 Turbulence quantification

We show in Table 1 turbulence quantities obtained via PIV analysis and averaged for each sequence. Fig.

S1 shows these quantities as a function of time during the entire measured period. The evolution of the energy dissipation rate ε after the pass of the grid was estimated from the Eulerian second-order longitudinal velocity structure function $D_{LL} = \langle (\Delta u_r)^2 \rangle$ where the brackets indicate ensemble average and where $\Delta u_r = [\mathbf{u}(\mathbf{x}, t) - \mathbf{u}(\mathbf{x} + \mathbf{r}, t)] \cdot \mathbf{r} / \|\mathbf{r}\|$ is the longitudinal velocity difference between two particles separated by a distance r . For isotropic turbulence, in the inertial range, $D_{LL} = C_K (\varepsilon r)^{2/3}$ where $C_K \cong 2.1$ is the universal Kolmogorov constant. The Kolmogorov length scale $\eta = (\nu^3/\varepsilon)^{1/4}$ and time scale $\tau_\eta = (\nu/\varepsilon)^{1/2}$, where ν is the kinematic viscosity of the fluid, range from 0.26 mm and 0.07 s in S1 to 0.42 mm and 0.17 s in S5, respectively. They were directly obtained from ε estimated via D_{LL} . The root mean square of the velocity fluctuations $\sigma_u = (1/2 [\langle (u'_x)^2 \rangle + \langle (u'_y)^2 \rangle])^{1/2}$ ranges from approx. 26 mm/s in S1 to 16 mm/s in S5. The integral length scale L , estimated via the integral of the autocorrelation function of the longitudinal velocity fluctuations, increases from 50 mm in S1 to 104 mm in S5. The Taylor microscale was estimated as $\lambda = \sigma_u (15\nu/\varepsilon)^{1/2}$ and increases from 10.4 mm in S1 to 22 mm in S5. As indicated above, the turbulence is strong in the first sequences because the goal is to test for the emergence of preferential concentration due to the conventional Stokes number St of copepods, which is close to unity in S1. Indeed, previous studies have shown that the intensity of the clustering due to St tends to increase with the Reynolds number [53]. Turbulence quantities in the last sequences are within the range considered in previous laboratory and theoretical studies of plankton motion in turbulence [68, 70] and observed in coastal environments [50]. They are appropriate to detect clustering due to swimming behavior. In these sequences, the velocity fluctuations are lower than the velocity reached by copepods during jumps [42], which indicates that the turbulence intensity is not too strong with respect to the swimming capabilities of the organisms, while the shear rate due to velocity gradients is still large enough to trigger escape reactions. Indeed, we estimate an average value for the shear rate as $\gamma = (\varepsilon/\nu)^{1/2}$ [54] and obtain $\gamma = 5.75 \text{ s}^{-1}$ in S5. This value is higher than the threshold, estimated at approx. 3 s^{-1} , needed to trigger escape jumps in *E. affinis* [6]. Finally, we verify that our flow is satisfactory isotropic and homogeneous. The isotropy coefficient, defined as the ratio of the standard deviation of the flow velocity along the two dimensions, ranges from approx. 0.89 at the beginning of S1 to 0.79 at the end of S5. The standard deviation of the turbulent kinetic energy is no larger than 10 % of the average turbulent kinetic energy.

3.2 Swimming velocity

We start our analysis by considering the velocity of copepods in calm water and turbulence to ensure that our observations align with previous results from the lit-

erature. In particular, we verify the presence of jumps in turbulence, a prerequisite for the emergence of clustering due to behavior. We show in Fig. 2A the PDF of the magnitude of the velocity of copepods swimming in calm water $u_{l,c}$. The shape of $P(u_{l,c})$ is in good agreement with previous experimental observations of copepod motion [45]. It is consistent with the swimming behavior of many species of calanoid copepods, including *E. affinis*, that alternate periods of slow swimming with frequent jumps [29]. The bulk of the distribution is observed for $u_{l,c} < 10 \text{ mm/s}$. It corresponds to the slow forward motion that derives from the creation of feeding currents accomplished by the vibration of the cephalic appendages. Above this value, the tail of the distribution corresponds to velocities reached during jumps. To illustrate the strong intermittency in the motion of copepods, we show in Fig. 2B a subset of trajectories color-coded with $u_{l,c}$. These trajectories were recorded in calm water, under infrared light, in the absence of any visual or hydrodynamic perturbations. Fig. 2C shows the time series of $u_{l,c}$ for one representative trajectory from this subset. Frequent velocity bursts are clearly visible, separated by periods of slow motion. Because their amplitude is moderate and restricted to a few tens of millimeters per second only (approx. 40 to 60 mm/s in our measurements), these velocity bursts are often referred to as relocation jumps to distinguish them from the escape jumps performed by copepods in response to a danger, for instance a nearby hydrodynamic disturbance or a sudden change in light intensity [32]. Escape jumps are much faster than relocation jumps. Previous measurements have shown that in *E. affinis*, escape jumps triggered by flow signals reach velocities between 100 and 150 mm/s [6, 45], whereas relocation jumps are limited to a few tens of mm/s [42]. Finally, we note that the shape of the jumps in our measurements is comparable with that observed in an earlier work for the same species [1]. After a very sharp increase, $u_{l,c}$ relaxes exponentially due to drag. Following [1], we estimate the mean decaying time τ_J by fitting the exponential function ue^{-t/τ_J} to the decaying part of the jump velocity. We obtain $\tau_J \cong 17 \text{ ms}$, which corresponds to $0.24 \tau_\eta$ in S1 and $0.1 \tau_\eta$ in S5.

We now examine the behavioral response of copepods to a sudden increase in turbulence intensity caused by the pass of the grid. Fig. 2D shows the ratio of the PDF of the velocity magnitude of living copepods swimming in turbulence $u_{l,t}$ to that of dead copepods passively transported by the flow $u_{d,t}$. The ratio is close to unity in S1, indicating that, immediately after grid pass, $u_{l,t}$ is determined mostly by the hydrodynamic conditions. This result shows that in strong turbulence, copepods are not able to swim independently of the flow as they would do in weaker turbulence [42]. As turbulence intensity decreases, the motion of living copepods is characterized by a substantial increase in the frequency of large velocities (from 50 to 150 mm/s), as indicated by a ratio $u_{l,t}/u_{d,t} \cong 3$ at $u = 125 \text{ mm/s}$ in S4 and S5. Velocities within this interval correspond

Table 1 Time- and space-averaged turbulence quantities within the investigation volume, for each sequence

	ε (m ² /s ³)	λ (mm)	L (mm)	η (mm)	τ_η (s)	u_η (mm/s)	σ_u (mm/s)	Re_λ
S1	2.70E-04	10.42	50.17	0.26	0.07	3.95	26.32	269
S2	7.64E-05	14.78	68.22	0.34	0.12	2.94	18.88	277
S3	3.64E-05	20.05	90.63	0.41	0.17	2.45	15.65	313
S4	3.35E-05	21.67	102.78	0.42	0.17	2.41	15.67	340
S5	3.31E-05	22.01	104.5	0.42	0.17	2.4	16.31	359

ε is the dissipation rate, $\lambda = \sigma_u (15\nu/\varepsilon)^{1/2}$ is the Taylor microscale, L is the integral length scale, $\eta = (\nu^3/\varepsilon)^{1/4}$ is the Kolmogorov length scale, $\tau_\eta = (\nu/\varepsilon)^{1/2}$ is the Kolmogorov time scale, $u_\eta = (\nu\varepsilon)^{1/4}$ is the Kolmogorov velocity scale, σ_u is the standard deviation of the turbulent velocity, and $Re_\lambda = \sigma_u \lambda/\nu$ is the Taylor-scale Reynolds number

to escape jumps rather than relocation jumps, which suggests that copepods perform more frequent escape jumps when exposed to strong and sudden turbulence. The gradual increase in the frequency of large velocities does not necessarily indicate that copepods perform more and more escape jumps. It indicates that these escape jumps become more and more visible as turbulence weakens.

The contribution of escape jumps triggered by hydrodynamic signals in the emergence of patchiness in the spatial distribution of copepods was recently investigated via numerical simulations [1]. Clustering was observed over a range of values u_J/u_η where u_J is the jump amplitude and u_η the Kolmogorov velocity scale, and was maximal for $\gamma_T \cong 0.5\tau_\eta^{-1}$ where γ_T is the threshold in shear rate above which copepods jump. Under our hydrodynamic conditions, taking $\gamma_T = 3\text{ s}^{-1}$ as previously measured for *E. affinis* [6], we obtain $\gamma_T = 0.51\tau_\eta^{-1}$ in S4 and S5. We estimate $u_J = 125\text{ mm/s}$ the average amplitude of escape jumps triggered by strong turbulence (Fig. 2D) and find $u_J/u_\eta \cong 52$ in S4 and S5. These values are within the range conducive to clustering in the numerical simulations of [1]. Therefore, one may expect copepods swimming in turbulence to concentrate within low shear rate regions of the flow because of their escape jumps, leading to behavior-induced preferential concentration.

3.3 Voronoï analysis

We show in Fig. 3A, as an illustration of the type of data gathered during the measurements, the trajectories of living copepods in turbulence corresponding to one sequence (approx. 2.33 s) of one replicate. Fig. 3B shows a subset of three-dimensional Voronoï cells for one single time step of the same sequence. Voronoï diagrams were calculated for each time step and then pooled for each sequence across replicates.

For inert carcasses, the PDF of the normalized volume of the Voronoï cells remains very close to that of particles distributed as a random Poisson process (Fig. 4A), even when turbulence is intense. There are also no clear differences between sequences S1 and S5. The slight deviation at small and large values of $V/\langle V \rangle$ is negligible when compared to that of particles with a larger St , for instance heavy particles or air bubbles

in turbulent flows, for which the PDF clearly departs from a random Poisson process distribution [21, 47, 62]. This implies that particle finite size, slight inertia, and elongated shape do not lead to substantial clustering of copepods in turbulence, at least for the species and range of parameters investigated in this study. A similar pattern is observed for living copepods swimming in turbulence, with no substantial departure from the PDF of randomly distributed particles and no difference between sequences S1 and S5 (Fig. 4B). It thus appears that the motility of copepods in turbulence does not result in their local accumulation within regions of the flow. Finally, we note the emergence of patchiness in the spatial distribution of copepods swimming in calm water, with a slightly higher probability of clusters and voids (low and high values of $V/\langle V \rangle$, respectively) than for randomly distributed particles (Fig. 4C). We attribute this phenomenon to encounters mediated by olfactory orientation and hydrodynamic interactions.

4 Discussion

The contribution of turbulence and motility in the emergence of patchiness has been well studied in phytoplankton, via laboratory observations [15] but mostly via numerical simulations that couple the behavior of the cells and the hydrodynamic forces they experience [7, 15]. There is much less information on preferential concentration in zooplankton because of the difficulties of tracking a sufficiently large number of organisms swimming in turbulence. This lack of data limits our ability to understand the mechanisms at play in this phenomenon and its prevalence in the environment.

Pioneering theoretical work and numerical simulations have suggested that clustering in zooplankton could result from the interactions between turbulence and the organisms owing to finite-size and density effects [55, 58]. Particles that have finite inertia often do not follow fluid trajectories, which leads to the emergence of preferential concentration: they spread non-uniformly and form clusters where their local concentration is higher than in nearby regions. In the idealized case of homogeneous isotropic turbulence, preferential concentration manifests itself in the form of small-scale clustering. Particles accumulate within transient, local-

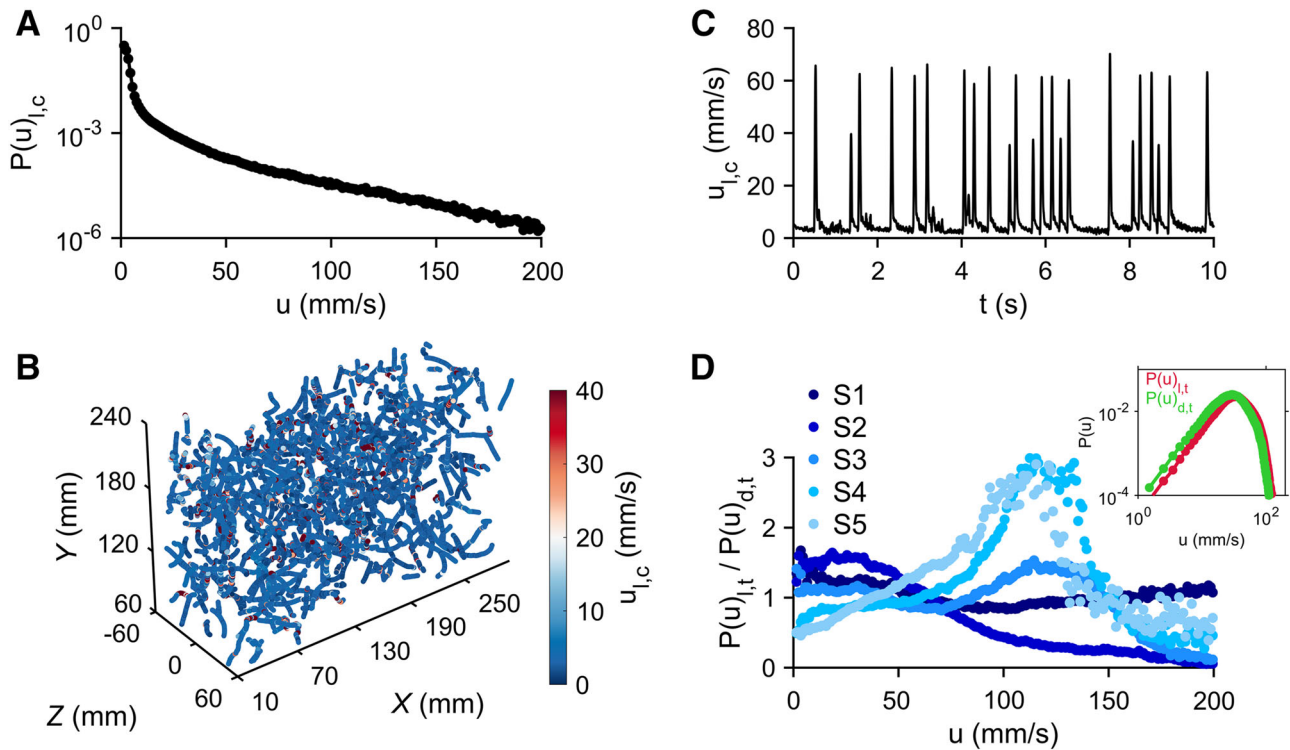


Fig. 2 Copepod velocity in calm water and turbulence. **A** PDF of the magnitude of the velocity of copepods swimming in calm water. All sequences have been combined since there is no turbulence decay. **B** Subset of trajectories of copepods swimming in calm water, color-coded with the magnitude of the velocity. Copepods alternate periods of slow swimming ($u_{l,c} < 10$ mm/s) with frequent relocation jumps ($u_{l,c} < 10$ mm/s). **C** Time series of $u_{l,c}$ for one representative trajectory from the same subset. At our recording frequency, most jumps have an amplitude lower than approx.

60 mm/s. We refer to these velocity bursts as *relocation jumps* to differentiate them from the much more powerful escape jumps. **D** Ratio of the PDF of the magnitude of the velocity of living copepods swimming in turbulence $u_{l,t}$ to that of dead copepods in turbulence $u_{d,t}$, for sequences S1 to S5. The inset shows $P(u)_{l,t}$ (red) and $P(u)_{d,t}$ (green) to emphasize the shift in the distribution toward larger velocities (approx. 125 mm/s). These velocities correspond to escape jumps triggered by strong turbulence

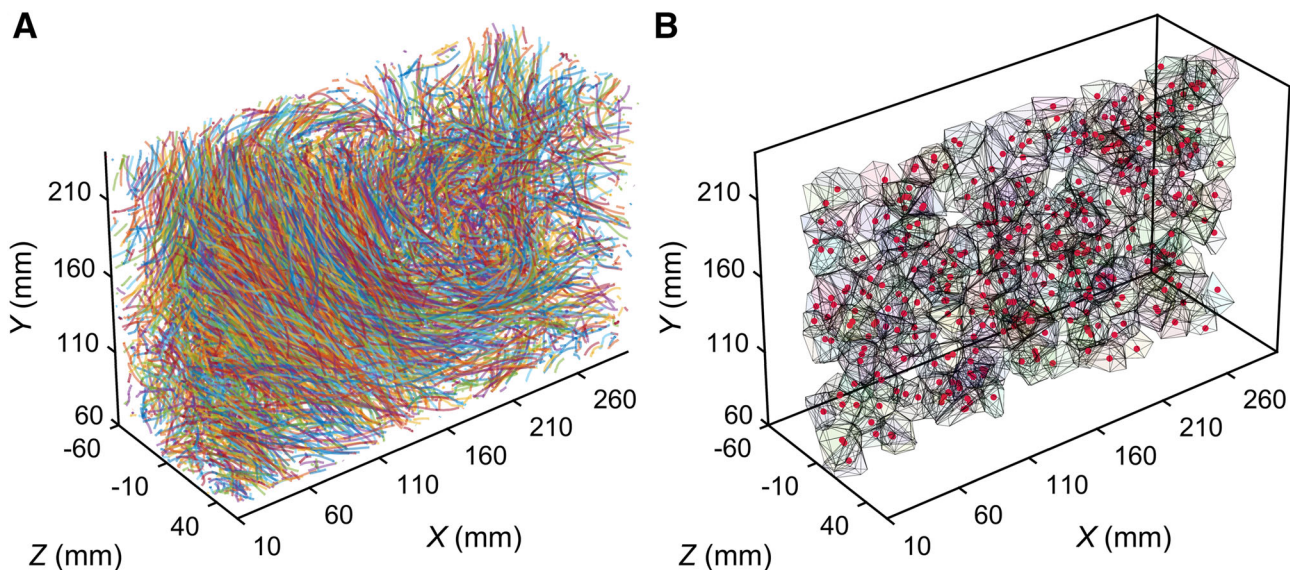


Fig. 3 Three-dimensional Voronoi analysis. **A** Subset of trajectories of copepods swimming in turbulence, corresponding to one single sequence of one recording. **B** Illustration of three-dimensional Voronoi cells. For clarity, we

only show cells that are entirely contained within a 40 mm thick slice in the middle of the volume and the associated copepod positions (red dots), for one single time step of the same sequence

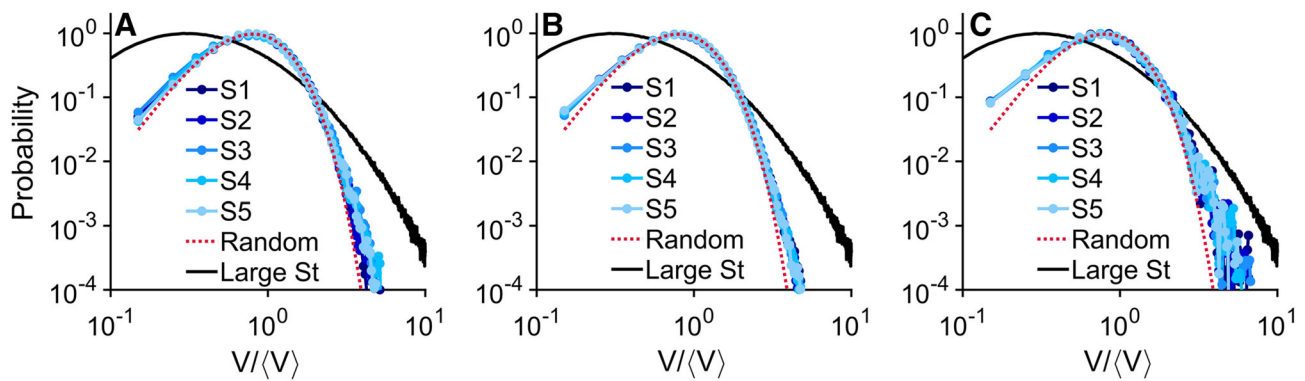


Fig. 4 Probability density functions of the normalized volume of the Voronoi cells. **A** Dead copepods in turbulence. **B** Living copepods in turbulence. **C** Living copepods in calm water. The dashed red line is the prediction for a random Poisson process [20]. For living and dead copepods in turbulence, the probability density functions deviate from a Poisson process for all sequences S1 to S5. However, the deviation appears to be negligible compared to that of particles with a larger St [47,62]. To illustrate this difference,

ized zones of high particle density that correspond to zones of high strain rate for inertial particles and to zones of high vorticity for bubbles, separated by voids where particle concentration is low. In the case of active particles, small-scale clustering can also result from the accumulation of the organisms into specific regions of the flow because of their behavioral response to hydrodynamic signals generated by turbulence. Indeed, copepods react to hydrodynamic perturbations by performing strong escape jumps with very short latency [9,32]. Numerical simulations have shown that, under certain behavioral parameters and flow conditions, copepods may accumulate into low shear rate regions of the flow by jumping away from high shear rate regions [1,2]. By means of a high-performance particle tracking technique and Voronoi analysis, we have studied the spatial distribution of a widespread calanoid copepod in a laboratory setup that creates quasi homogeneous and isotropic turbulence and found that they do not exhibit preferential concentration. Neither inertial effects or motility combined with inertia resulted in a substantial departure of their spatial distribution from that of randomly distributed particles, over the range of turbulence intensity tested.

Our results agree with previous experimental investigations from the field of turbulence research reporting on the absence of significant clustering of inert particles with a density comparable to that of the carrier fluid and a size larger than or comparable to the dissipation scale η of the flow. Heavy and light inertial particles that are much smaller than η do cluster, as well as large heavy particles [27,46,47,62]. Conversely, finite-size particles that are neutrally buoyant or with a density close to that of the fluid do not tend to cluster [21,43,67], even though their dynamics may differ from that of tracers [8,64]. The conventional Stokes number, based on the particle viscous relaxation time and the

we show the probability density function of $V/\langle V \rangle$ for heavy particles ($St = 3.3$) at a comparable Re_λ from the measurements of [47] (black curve). The clustering of heavy particles is significant, while the distribution of $V/\langle V \rangle$ for inert and living copepods in turbulence resembles that of a RPP. The deviation is more important for living copepods in calm water, reflecting the probable contribution of olfactory orientation in bringing organisms in close proximity

Kolmogorov time scale, is not sufficient to describe the dynamics of such particles in turbulence. This limitation is well known and was previously illustrated both for the spatial distribution of the particles [21] and for dynamical properties such as their acceleration [52,67]. For these particles, a modified Stokes number was previously suggested, based on the eddy turnover time at the scale of the particle and including a correction due to the particle Reynolds number [67]. This modified Stokes number is smaller than the conventional Stokes number (and better describes the behavior of finite-size but not inertial particles in turbulence. In our measurements, the conventional Stokes number of dead copepods is approx. 0.8 in S1 while the modified Stokes number is approx. 0.14. Finally, we note that the lack of preferential concentration of inert carcasses in our study is in good agreement with an earlier experimental investigation that reported on no significant clustering of dead copepods in stationary homogeneous isotropic turbulence, using the correlation function of the particle concentration [43].

An important point that emerges from the Voronoi analysis is the absence of preferential concentration caused by the behavioral response of copepods to turbulence. The reasons behind the disparity between our measurements and earlier numerical simulations [1,2] are unknown but may include different flow conditions. The shear rate threshold required to trigger escape jumps in copepods varies between species. It was estimated at approx. 2 to 3 s^{-1} for *E. affinis* [6,63], which is lower than the mean shear rate in our flow ($\dot{\gamma} = 5.75 s^{-1}$ in S5). The ratio $u_{l,t}/u_{d,t} \cong 3$ for $u = 125$ mm/s (Fig. 2D) confirms that copepods performed strong escape jumps in our measurements; however it is possible that the limited time scale (approx. 12 s) did not give enough time for the copepods to accumu-

late within intermittent regions of low shear rate. We note that a recent experimental study found no clustering of copepods swimming in stationary turbulence over several minutes [43]. It is also possible that copepods did not react in our measurements in the same way as in the simulation of [1]. In particular, copepods are able to maintain some degree of correlation in the direction of successive jumps in turbulence, which may have prevented their reorientation and accumulation outside regions of high shear rate [42]. Further work is required to understand whether the difference in flow conditions (transient versus stationary turbulence) and certain unexpected features in the swimming behavior of copepods have contributed to the deviation between numerical modeling and experimental data. Finally, we observed a slight tendency of *E. affinis* to cluster in calm water. We attribute this enhanced local concentration to the existence of interactions between organisms, mediated by pheromone communication at the scale of a few centimeters and by hydrodynamic signals at the scale of a few millimeters. In calm hydrodynamic conditions, male *E. affinis* can locate females at a distance of several centimeters via the pheromone trail left behind females. Males then swim along the pheromone gradient until contact [30]. This behavior is likely to increase the time spent by two copepods in close proximity. Males also lunge toward nearby conspecifics upon sensing the hydrodynamic perturbations they generate while swimming. This occurs at a separation distance of approx. 5 mm [43] and may increase the probability of observing two organisms in close vicinity, leading to local accumulation.

The motion of zooplankton is shaped by the coupling between their swimming behavior, transport due to turbulence, and effects due to hydrodynamic forces acting on their body [41]. Obtaining information on this coupling is necessary to explain and predict a variety of important processes that affect their life, such as reproduction and predation [2, 49]. For instance, the nonlinear velocity gradients experienced by anisotropic zooplankton larger than the Kolmogorov scale as they swim or are entrained in turbulence influence their rotation rate [5]. This may in turn affect their orientation and their ability to detect an approaching predator [48]. Here, we show that neither physical effects (due to the density difference between the organism and the fluid, to its finite size and to its elongated shape) nor behavior result in substantial preferential concentration of zooplankton in turbulence. This finding has important ecological implications, because it means that small-scale clustering is unlikely to lead to higher encounter rates between organisms with similar morphology, and therefore that it does not increase significantly mating success or predation rates. The lack of preferential concentration in the spatial distribution of plankton also makes it possible to develop simpler encounter rate models for plankton in turbulence. Indeed, in the absence of clustering, the collision kernel reduces to the clearance rate that originates from the contribution of organism motility and transport by turbulence, and to the collision efficiency that accounts for behavioral

interactions between organisms at short separation distance [43].

The aim of this study was to test for the existence and extent of preferential concentration due to inertia and escape jumps by targeting flow conditions conducive to its emergence, not to investigate the behavioral response of copepods to various intensities of turbulence. How copepods react to turbulence has already been studied in earlier experimental works, including their response to different conditions of stationary turbulence more representative of their natural environment [45, 70]. We also emphasize that our goal was to quantify plankton accumulation in quasi-homogeneous isotropic turbulence representative of flow conditions found in the pelagic ocean. The contribution of turbophoresis in the emergence of preferential concentration in the case of inhomogeneous turbulence is outside the scope of this work. Finally, we stress that the time and spatial scales of clustering considered in this study are on the order of a few seconds and millimeters to centimeters. Plankton aggregation occurs over a range of scales from small to large. At small scale, it is often caused by the coupling between hydrodynamic forces, the shape and inertia of the organisms, and their behavior in the case of motile plankton. The formation of plankton patches at the mesoscale may be caused by a variety of processes that are not the topic of this work, such as gyrotactic trapping or displacements toward favorable areas [17, 25, 28].

Our measurements complement current efforts to unravel the nature and ecological consequences of the coupling between turbulence and motility in the plankton. They provide experimental evidence that can be used to validate and parametrize numerical simulations of flow-behavior interactions at small scales, in particular encounter rates [1]. Such simulations offer the opportunity to study important processes mediated by turbulence and motility at a resolution often difficult to achieve in laboratory measurements, for instance in terms of flow field resolution.

Supplementary information The online version contains supplementary material available at <https://doi.org/10.1140/epje/s10189-022-00167-5>.

Acknowledgements We thank S. Souissi (Lille University) for providing the copepods and phytoplankton and the *Communauté d'Agglomération du Boulonnais* for supporting the implementation of a large-scale copepod rearing pilot project. We are thankful to C. Bialais and D. Menu (LOG) for transporting the copepods to IMFT and for their help during the measurements, and the past and current members of the group of S. Souissi for maintaining the continuous plankton cultures. We thank J.-D. Barron (IMFT) for building the experimental setup and the students from *École Navale* for assisting with the PIV measurements. We acknowledge the CNRS Research Federation FERMaT (FR 3089) for giving access to the shared 3D-PTV and time-resolved tomographic PIV system, and the CNRS MITI program for financial support.

Funding This work was supported by the *Laboratoire Associé International MULTIFAQUA* between Lille University and National Taiwan Ocean University and by a STaRS fellowship from the *Région Hauts-de-France* (to F.-G. M.).

Author contribution statement

F.-G. M., O. P., S. C. and E. C. designed experiments and performed measurements. F.-G. M. analyzed the data and wrote the manuscript. O. P., S. C. and E. C. helped editing the manuscript. All authors contributed to funding acquisition.

Declarations

Conflict of interest The authors declare no competing interests.

References

1. H. Ardeshiri, I. Benkeddad, F.G. Schmitt, S. Souissi, F. Toschi, E. Calzavarini, Lagrangian model of copepod dynamics: clustering by escape jumps in turbulence. *Phys. Rev. E* **93**, 043117 (2016)
2. H. Ardeshiri, F.G. Schmitt, S. Souissi, F. Toschi, E. Calzavarini, Copepods encounter rates from a model of escape jump behaviour in turbulence. *J. Plankton Res.* **39**(6), 878–890 (2017)
3. G. Beaugrand, K.M. Brander, J.A. Lindley, S. Souissi, P.C. Reid, Plankton effect on cod recruitment in the North Sea. *Nature* **426**, 661–664 (2003)
4. J. Bec, L. Biferale, M. Cencini, A. Lanotte, S. Musacchio, F. Toschi, Heavy particle concentration in turbulence at dissipative and inertial scales. *Phys. Rev. Lett.* **98**, 084502 (2007)
5. A.D. Bordoloi, E. Variano, G. Verhille, Lagrangian time scale of passive rotation for mesoscale particles in turbulence. *Front. Mar. Sci.* **7**, 473 (2020)
6. C.J. Bradley, J.R. Strickler, E.J. Buskey, P.H. Lenz, Swimming and escape behavior in two species of calanoid copepods from nauplius to adult. *J. Plankton Res.* **35**(1), 49–65 (2013)
7. R.E. Breier, C.C. Lalescu, D. Waas, M. Wilczek, M.G. Mazza, Emergence of phytoplankton patchiness at small scales in mild turbulence. *Proc. Natl. Acad. Sci. USA* **115**(48), 12112–12117 (2018)
8. R.D. Brown, Z. Warhaft, G.A. Voth, Acceleration statistics of neutrally buoyant spherical particles in intense turbulence. *Phys. Rev. Lett.* **103**, 194501 (2009)
9. E.J. Buskey, P.H. Lenz, D.K. Hartline, Escape behavior of planktonic copepods in response to hydrodynamic disturbances: high speed video analysis. *Mar. Ecol. Prog. Ser.* **235**, 135–146 (2002)
10. S.W. Coleman, J.C. Vassilicos, A unified sweep-stick mechanism to explain particle clustering in two- and three-dimensional homogeneous, isotropic turbulence. *Phys. Fluids* **21**, 113301 (2009)
11. S. Das, B. Ouddane, J.-S. Hwang, S. Souissi, Intergenerational effects of resuspended sediment and trace metal mixtures on life cycle traits of a pelagic copepod. *Environ. Pollut.* **267**, 115460 (2020)
12. F. De Lillo, M. Cencini, W.M. Durham, M. Barry, R. Stocker, E. Climent, G. Boffetta, Turbulent fluid acceleration generates clusters of gyrotactic microorganisms. *Phys. Rev. Lett.* **112**(4), 044502 (2014)
13. D. Devreker, S. Souissi, J.C. Molinero, D. Beyrend-Dur, F. Gomez, J. Forget-Leray, Tidal and annual variability of the population structure of *Eurytemora affinis* in the middle part of the Seine Estuary during 2005. *Estuar. Coast. Shelf Sci.* **89**(4), 245–255 (2010)
14. D. Devreker, S. Souissi, J.C. Molinero, F. Nkubito, Trade-offs of the copepod *Eurytemora affinis* in megatidal estuaries: insights from high frequency sampling in the Seine estuary. *J. Plankton Res.* **30**(12), 1329–1342 (2008)
15. W.M. Durham, E. Climent, M. Barry, F. De Lillo, G. Boffetta, M. Cencini, R. Stocker, Turbulence drives microscale patches of motile phytoplankton. *Nat. Commun.* **4**, 2148 (2013)
16. W.M. Durham, J.O. Kessler, R. Stocker, Disruption of vertical motility by shear triggers formation of thin phytoplankton layers. *Science* **323**(5917), 1067–1070 (2009)
17. W.M. Durham, R. Stocker, Thin phytoplankton layers: characteristics, mechanisms, and consequences. *Ann. Rev. Mar. Sci.* **4**, 177–207 (2012)
18. M. Elhimer, O. Praud, M. Marchal, S. Cazin, R. Bazile, Simultaneous PIV/PTV velocimetry technique in a turbulent particle-laden flow. *J. Visualization* **20**, 289–304 (2016)
19. D. Elmi, D.R. Webster, D.M. Fields, Response of the copepod *Acartia tonsa* to the hydrodynamic cues of small-scale, dissipative eddies in turbulence. *J. Exp. Biol.* **224**(3), 237297 (2021)
20. J.-S. Ferenc, Z. Néda, On the size distribution of Poisson Voronoi cells. *Phys. A* **385**(2), 518–526 (2007)
21. L. Fiabane, R. Zimmermann, R. Volk, J.-F. Pinton, M. Bourgoin, Clustering of finite-size particles in turbulence. *Phys. Rev. E* **86**, 035301(R) (2012)
22. I. Fouxon, A. Leshansky, Phytoplankton's motion in turbulent ocean. *Phys. Rev. E* **92**, 013017 (2015)
23. P.J.S. Franks, B.G. Inman, J.A. MacKinnon, M.H. Alford, A.F. Waterhouse, Oceanic turbulence from a planktonic perspective. *Limnol. Oceanogr.* (2022). <https://doi.org/10.1002/lno.11996>
24. H.L. Fuchs, G.P. Gerbi, E.J. Hunter, A.J. Christman, Waves cue distinct behaviors and differentiate transport of congeneric snail larvae from sheltered versus wavy habitats. *Proc. Natl. Acad. Sci. USA* **115**(32), E7532–E7540 (2018)
25. S. Gallager, H. Yamazaki, C.S. Davis, Contribution of fine-scale vertical structure and swimming behavior to formation of plankton layers on Georges Bank. *Mar. Ecol. Prog. Ser.* **267**, 27–43 (2004)
26. M. Gibert, H. Xu, E. Bodenschatz, Where do small, weakly inertial particles go in a turbulent flow? *J. Fluid Mech.* **698**, 160–167 (2012)
27. M. Guala, A. Liberzon, K. Hoyer, A. Tsinober, W. Kinzelbach, Experimental study on clustering of large particles in homogeneous turbulent flow. *J. Turbul.* **9**, N34 (2008)
28. L.S. Incze, D. Hebert, N. Wolff, N. Oakey, D. Dye, Change in copepod distributions associated with

- increased turbulence from wind stress. *Mar. Ecol. Prog. Ser.* **213**, 229–240 (2001)
29. H. Jiang, T. Kiørboe, The fluid dynamics of swimming by jumping in copepods. *J. R. Soc. Interface* **8**, 1090–1103 (2011)
 30. S.K. Katona, Evidence for sex pheromones in planktonic copepods. *Limnol. Oceanogr.* **18**(4), 574–583 (1973)
 31. D.G. Kimmel, M.R. Roman, Long-term trends in mesozooplankton abundance in Chesapeake Bay, U.S.A.: influence of freshwater input. *Mar. Ecol. Prog. Ser.* **267**, 71–83 (2004)
 32. T. Kiørboe, A. Andersen, V.J. Langlois, H.H. Jakobsen, Unsteady motion: escape jumps in planktonic copepods, their kinematics and energetics. *J. R. Soc. Interface* **7**, 1591–1602 (2010)
 33. T. Kiørboe, E. Saiz, A. Visser, Hydrodynamic signal perception in the copepod *Acartia tonsa*. *Mar. Ecol. Prog. Ser.* **179**, 97–111 (1999)
 34. T. Knutsen, W. Melle, L. Calise, Determining the mass density of marine copepods and their eggs with a critical focus on some of the previously used methods. *J. Plankton Res.* **23**(8), 859–873 (2001)
 35. D.M. Lewis, T.J. Pedley, Planktonic contact rates in homogeneous isotropic turbulence: Theoretical predictions and kinematic simulations. *J. Theor. Biol.* **205**(3), 377–408 (2000)
 36. A. Liberzon, B. Lüthi, M. Holzner, S. Ott, J. Berg, J. Mann, On the structure of acceleration in turbulence. *Physica D* **241**(3), 208–215 (2012)
 37. Lüthi B. (2002) Some aspects of strain, vorticity and material element dynamics as measured with 3D particle tracking velocimetry in a turbulent flow. Doctoral thesis, ETH Zurich, Switzerland. <https://doi.org/10.3929/ethz-a-004496218>
 38. H.-G. Maas, A. Gruen, D. Papantoniou, Particle tracking in three-dimensional turbulent flows. Part I: Photogrammetric determination of particle coordinates. *Exp. Fluids* **15**(2), 133–146 (1993)
 39. N.A. Malik, T. Dracos, D. Papantoniou, Particle tracking velocimetry in three-dimensional turbulent flows. Part II: Particle tracking. *Exp. Fluids* **15**(4–5), 279–294 (1993)
 40. Marchioli C., Bhatia H., Dotto D. (2021) Influence of particle anisotropy and motility on preferential concentration in turbulence. In: Deville M. et al. (eds) *Turbulence and Interactions. Notes on Numerical Fluid Mechanics and Multidisciplinary Design*, volume 149
 41. M.A. McManus, C.B. Woodson, Plankton distribution and ocean dispersal. *J. Exp. Biol.* **215**(6), 1008–1016 (2012)
 42. F.-G. Michalec, I. Fouxon, S. Souissi, M. Holzner, Zooplankton can actively adjust their motility to turbulent flow. *Proc. Natl. Acad. Sci. USA* **114**(52), E11199–E11207 (2017)
 43. F.-G. Michalec, I. Fouxon, S. Souissi, M. Holzner, Efficient mate finding in planktonic copepods swimming in turbulence. *Elife* **9**, e62014 (2020)
 44. F.-G. Michalec, F.G. Schmitt, S. Souissi, M. Holzner, Characterization of intermittency in zooplankton behaviour in turbulence. *Eur. Phys. J. E* **388**, 108 (2015)
 45. F.-G. Michalec, S. Souissi, M. Holzner, Turbulence triggers vigorous swimming but hinders motion strategy in planktonic copepods. *J. R. Soc. Interface* **12**, 20150158 (2015)
 46. R. Monchaux, M. Bourgoïn, A. Cartellier, Preferential concentration of heavy particles: A Voronoï analysis. *Phys. Fluids* **22**, 103304 (2010)
 47. M. Obligado, T. Teitelbaum, A. Cartellier, P. Mininni, M. Bourgoïn, Preferential concentration of heavy particles in turbulence. *J. Turbul.* **15**(5), 293–310 (2014)
 48. H.L. Pécseli, J.K. Trulsen, Plankton's perception of signals in a turbulent environment. *Adv. Phys.: X* **1**(1), 20–34 (2016)
 49. H.L. Pécseli, J.K. Trulsen, J.E. Stiansen, Sundby, Feeding of plankton in a turbulent environment: A comparison of analytical and observational results covering also strong turbulence. *Fluids* **5**(1), 37 (2020)
 50. H.L. Pécseli, J.K. Trulsen, J.E. Stiansen, S. Sundby, P. Fossum, Feeding of plankton in turbulent oceans and lakes. *Limnol. Oceanogr.* **64**(3), 1034–1046 (2019)
 51. N. Pujara, M.A.R. Koehl, E.A. Variano, Rotations and accumulation of ellipsoidal microswimmers in isotropic turbulence. *J. Fluid Mech.* **838**, 356–368 (2018)
 52. N.M. Qureshi, U. Arrieta, C. Baudet, A. Cartellier, Y. Cagne, M. Bourgoïn, Acceleration statistics of inertial particles in turbulent flow. *Eur. Phys. J. B* **66**, 531–536 (2008)
 53. W.C. Reade, L.R. Collins, Effect of preferential concentration on turbulent collision rates. *Phys. Fluids* **12**, 2530 (2000)
 54. D. Saha, M.U. Babler, M. Holzner, M. Soos, B. Lüthi, A. Liberzon, W. Kinzelbach, Breakup of finite-size colloidal aggregates in turbulent flow investigated by 3D particle tracking velocimetry. *Langmuir* **32**, 155–65 (2016)
 55. F.G. Schmitt, L. Seuront, Intermittent turbulence and copepod dynamics: Increase in encounter rates through preferential concentration. *J. Mar. Syst.* **70**(3–4), 263–272 (2008)
 56. D. Sidler, F.-G. Michalec, M. Detert, M. Holzner, Three-dimensional tracking of the motion of benthic copepods in the free water and inside the transparent sediment bed of a laboratory flume. *Limnol. Oceanogr. Methods* **15**(2), 125–139 (2017)
 57. U. Sommer, R. Adrian, L. De Senerpont Domis, J.J. Elser, U. Gaedke, B. Ibelings, E. Jeppesen, M. Lürling, J.C. Molinero, W.M. Mooij, E. van Donk, M. Winder, Beyond the plankton ecology group (PEG) model: Mechanisms driving plankton succession. *Annu. Rev. Ecol. Evol. Syst.* **43**, 429–448 (2012)
 58. K.D. Squires, H. Yamazaki, Preferential concentration of marine particles in isotropic turbulence. *Deep Sea Res. Part I* **42**(11–12), 1989–2004 (1995)
 59. D.K. Steinberg, M.R. Landry, Zooplankton and the ocean carbon cycle. *Ann. Rev. Mar. Sci.* **9**, 413–444 (2017)
 60. S. Sundaram, L.R. Collins, Collision statistics in an isotropic particle-laden turbulent suspension. Part 1. Direct numerical simulations. *J. Fluid Mech.* **335**, 75–109 (1997)
 61. P. Sutherland, W.K. Melville, Field measurements of surface and near-surface turbulence in the presence of breaking waves. *J. Phys. Oceanogr.* **45**(4), 943–965 (2015)
 62. Y. Tagawa, J.M. Mercado, V.N. Prakash, E. Calzavarini, C. Sun, D. Lohse, Three-dimensional Lagrangian

- Voronoi analysis for clustering of particles and bubbles in turbulence. *J. Fluid Mech.* **693**, 201–215 (2012)
63. M. Viitasalo, T. Kiørboe, J. Flinkman, L.W. Pedersen, A.W. Visser, Predation vulnerability of planktonic copepods: consequences of predator foraging strategies and prey sensory abilities. *Mar. Ecol. Prog. Ser.* **175**, 129–142 (1998)
64. G.A. Voth, A. La Porta, A.M. Crawford, J. Alexander, E. Bodenschatz, Measurement of particle accelerations in fully developed turbulence. *J. Fluid Mech.* **469**, 121–160 (2002)
65. Willneff J. (2003) A spatio-temporal matching algorithm for 3D particle tracking velocimetry. Doctoral thesis, ETH Zurich, Switzerland. <https://doi.org/10.3929/ethz-a-004620286>.
66. A.M. Wood, W. Hwang, J.K. Eaton, Preferential concentration of particles in homogeneous and isotropic turbulence. *Int. J. Multiph. Flow* **31**(10–11), 1220–1230 (2005)
67. H. Xu, E. Bodenschatz, Motion of inertial particles with size larger than Kolmogorov scale in turbulent flows. *Physica D* **237**(14–17), 2095–2100 (2008)
68. H. Yamazaki, K.D. Squires, Comparison of oceanic turbulence and copepod swimming. *Mar. Ecol. Prog. Ser.* **144**, 299–301 (1996)
69. J. Yen, P.H. Lenz, D.V. Gassie, D.K. Hartline, Mechanoreception in marine copepods: electrophysical studies on the first antennae. *J. Plankton Res.* **14**(4), 495–512 (1992)
70. J. Yen, K.D. Rasberry, D.R. Webster, Quantifying copepod kinematics in a laboratory turbulence apparatus. *J. Mar. Syst.* **69**(3–4), 283–294 (2008)